Knight shifts and nuclear-spin-relaxation rates for two-dimensional models of CuO_2

N. Bulut, D. W. Hone, and D. J. Scalapino
Department of Physics, University of California, Santa Barbara, California 93106

N. E. Bickers
Department of Physics, University of Southern California, Los Angeles, California 90089
and Institute for Theoretical Physics, University of California, Santa Barbara, California 93106
(Received 17 August 1989)

Using spin-wave and random-phase-approximation expressions for the dynamic spin susceptibility of a two-dimensional CuO_2 lattice, we have calculated the NMR Knight shifts K and spin-relaxation rates T_1^{-1} at various nuclear sites for the insulating and metallic phases. Our results suggest that the observed differences in the NMR data taken on different sites are qualitatively consistent with a model that has strongly hybridized Cu($3d$)-O($2p\sigma$) orbitals. Within this picture, local antiferromagnetic correlations produced by on-site Coulomb interactions enhance the large-momentum part of the spin susceptibility. These correlations are then spatially filtered by the hyperfine form factors leading to different local-site behavior.

I. INTRODUCTION

NMR measurements of the Knight shifts K and the nuclear spin-relaxation rates T_1^{-1} provide important insight into the character of the low-energy spin fluctuations in the layered cuprates.[1-8] With doping, which moves the planar copper away from a formal chemical valence of Cu^{2+}, these materials can be changed from insulating to metallic and superconducting. Thus one can explore the spin fluctuations of these materials over a remarkably wide range of correlated electronic behavior. Furthermore, by studying the temperature dependence and anisotropy of K and T_1^{-1} on different sites (Cu, O, rare earth), one obtains local information. These materials are quasi-two-dimensional, and much of the attention has focused on the CuO_2 sheets which are a common feature. In the insulating state the Cu^{2+} spins in the CuO_2 layers are coupled antiferromagnetically by a superexchange interaction mediated by the intervening O. The exchange coupling between the layers is weak, and the neutron scattering data[9] above the 3D Néel ordering temperature have been well described in terms of a 2D spin-$\frac{1}{2}$ Heisenberg antiferromagnet.[10,11] In this case, the NMR relaxation at the Cu site reflects the strong antiferromagnetic fluctuations and their exponential growth (for a 2D system) as the temperature decreases (above T_N). In contrast, the oxygen nuclei, coupled via a transferred hyperfine interaction to adjacent Cu spins, have a form factor that suppresses the antiferromagnetic fluctuations, and the O relaxation rate would be expected to decrease as T is lowered.[12] The long-range antiferromagnetic correlations are observed[9] to be rapidly suppressed by doping with additional holes, and at a relatively small concentration of excess holes the system exhibits a metallic phase that becomes superconducting at sufficiently low temperatures. Above the superconducting transition temperature, the response at the planar Cu sites reflects[1,4] remanent 2D antiferromagnetic fluctuations, while the response at the planar O sites, and at the interplanar Y sites[6,8] (in YBaCuO) appears free-electron-like in character. The fact that below T_c the relaxation rate T_1^{-1} exhibits a dramatic decrease, associated with pairing, on both the Cu and O sites, as well as data on the electronic field gradient and Knight shift tensors,[5] suggest that the doped holes are formed from the strongly hybridized Cu($3d$)$-$O($2p\sigma$) orbitals. Within this picture the doped metallic state can be viewed as a strongly interacting quantum liquid, with a dynamic spin susceptibility that reflects the local correlations produced by the Coulomb interactions. The contrasting NMR behavior seen on the Cu, O, and Y sites is then found to arise from the different hyperfine form factors that act to spatially filter the spin susceptibility.

Motivated by this rich variety of phenomena and the increasing amount of high-quality experimental data, we felt it would be useful to carry out detailed calculations of K and T_1^{-1} using simple approximations for the dynamic spin susceptibility and various hyperfine form factors. The first approximation, based on a strong-coupling picture, uses the results of a spin-wave-like approximation to a Heisenberg exchange model[13-15] for the dynamic structure factor of the Cu spins. In this model, as in Ref. 12, the extra doped holes are assumed to act only to limit the spin-spin correlation length and the Cu moments remain the source of the hyperfine coupling. Our second approach involves a weak coupling RPA calculation of the spin susceptibility $\chi(\mathbf{q},\omega)$ for a 2D Hubbard model and for a 2D CuO_2 lattice. In the latter, three-band Hubbard, model the susceptibility has Cu and O site indices as well as $(\mathbf{q},\omega)$ dependence. We examine various hyperfine form factors involving coupling both to the Cu and to the O spins: (1) for the Cu nuclei, (a) an on site isotropic hyperfine coupling and (b) a combined anisotropic on site and an isotropic nearest-neighbor Cu transferred

hyperfine interaction; (2) for O nuclei, (a) nearest-neighbor isotropic transferred hyperfine coupling to Cu spins and (b) nearest-neighbor isotropic transferred hyperfine coupling to O spins; and (3) for Y nuclei, nearest-neighbor isotropic transferred hyperfine coupling to O spins.[8,16]

In Sec. II, we begin with the Heisenberg model. This is clearly appropriate in the insulating limit that has been treated by several authors,[12,17] and we discuss the relationship of our results to theirs. In Sec. III, RPA calculations of K and T_1^{-1} are presented for the 2D Hubbard model, and in Sec. IV similar results are presented for a three-band CuO_2 lattice model. Our goal is to understand what these simple approximate models for $\chi(\mathbf{q},\omega)$ imply for the NMR response, and how the various form factors act to filter $\chi(\mathbf{q},\omega)$. In Sec. V we conclude with some comparisons of the results obtained from these different models.

II. THE STRONG-COUPLING REGIME

As a model for the two-dimensional insulating system, we take a spin-$\frac{1}{2}$ Heisenberg Hamiltonian with the nearest-neighbor exchange

$$H=J\sum_{\langle ij\rangle}\mathbf{S}_i\cdot\mathbf{S}_j\ . \tag{2.1}$$

Here $J>0$ is the exchange strength and the sum is over all nearest-neighbor pairs of spins on a square lattice. This model has been shown to give excellent agreement with the neutron scattering data.[11] In the following we will set $\hbar=k_B=1$. The spin relaxation rate for a nucleus at site n (either the location of an electronic spin, or any other atomic site in the lattice) is then given[18,19] by

$$\frac{1}{T_1}=\frac{T}{N}\sum_{\mathbf{q}\nu}A_\nu^2(\mathbf{q})\frac{\mathrm{Im}\chi_{\nu\nu}(\mathbf{q},\omega_0)}{\omega_0}$$
$$=\frac{1}{2N}\sum_{\mathbf{q},\nu}A_\nu^2(\mathbf{q})S(\mathbf{q},\omega_0)\ , \tag{2.2}$$

where the relaxation mechanism is taken to be the hyperfine interaction

$$H_{\mathrm{hf}}=\sum_{j,\nu}A_\nu^{nj}I_n^\nu S_j^\nu\ . \tag{2.3}$$

The sum on ν in Eq. (2.2) is over components of the diagonal hyperfine tensor perpendicular to the applied magnetic field (assumed to be along a principal axis of that tensor), and $A(\mathbf{q})$ is the Fourier transform of the tensor A^{nj} defined in Eq. (2.3). We note that the sum on $\mathbf{q}$ is over the Brillouin zone of the full lattice. The susceptibility $\chi_{\nu\nu}$ is by symmetry independent of the Cartesian index ν, and is therefore just half of χ^{+-}, defined as the response to a rotating magnetic field, which will be used in the calculations of later sections: $2\chi_{\nu\nu}=\chi^{+-}$. The imaginary part of the susceptibility, $\mathrm{Im}\chi^{+-}(\mathbf{q},\omega_0)$ is related [as indicated in Eq. (2.2)] by a factor

$$(e^{\beta\omega}-1)/(2e^{\beta\omega})\approx\beta\omega/2$$

to the dynamic structure factor $S(\mathbf{q},\omega)$:

$$S(\mathbf{q},\omega_0)=\tfrac{1}{2}\int_{-\infty}^{\infty}dt\,e^{i\omega_0 t}\langle S_{\mathbf{q}}^+(t)S_{\mathbf{q}}^-(0)\rangle\ , \tag{2.4}$$

taken at the electronic Zeeman frequency, ω_0. This is far smaller than the characteristic frequency J of the spin dynamics, and in most cases can be taken as zero, but we will invoke it where necessary as a low-frequency cutoff. The time dependence of the spin operators is now governed only by the isotropic Heisenberg Hamiltonian, and the exact result for $S(\mathbf{q},\omega)$ is therefore independent of the Cartesian component of the spin operators used to define it:

$$\langle S^\nu(t)S^\nu(0)\rangle=\tfrac{1}{2}\langle S^+(t)S^-(0)\rangle$$

is independent of $\nu=x,y$, or z.

Several approximations have been proposed[11,13–15] for the dynamic structure factor $S(\mathbf{q},\omega)$ of this system at the low temperatures of interest ($T\ll J$). We make use here of the form given[20] by both a mean-field Schwinger boson theory[13] and by a constrained spin-wave theory:[14,15]

$$S(\mathbf{q},0)=\frac{2\pi}{3N}\sum_{\mathbf{k}}\frac{n_{\mathbf{k}}(n_{\mathbf{k}}+1)}{1-\eta^2\gamma_{\mathbf{k}}^2}\left[1-\tfrac{1}{2}\eta^2\gamma_{\mathbf{k}}^2\left[1+\frac{\gamma_{\mathbf{k}+\mathbf{q}}}{\gamma_{\mathbf{k}}}\right]\right]$$
$$\times\delta(\omega_{\mathbf{k}+\mathbf{q}}-\omega_{\mathbf{k}})\ , \tag{2.5}$$

where the excitation energies are given by

$$\omega_{\mathbf{k}}=\lambda(1-\eta^2\gamma_{\mathbf{k}}^2)^{1/2}\ ,$$
$$\gamma_{\mathbf{k}}=\tfrac{1}{2}(\cos k_x+\cos k_y)\ . \tag{2.6}$$

The factor λ sets the excitation energy scale, or the spin-wave velocity; at low temperatures it is approximately $2J$. The coefficient η, which determines the energy gap, is exponentially close to unity at low temperatures. In terms of the static spin correlation length ξ it is given as

$$1-\eta=1/(16\xi^2)\approx 0.37(T/J)^2e^{-3Z_\kappa\pi J/T}\ , \tag{2.7}$$

where $Z_\kappa\approx 0.23$ renormalizes the correlation length exponent. The Bose occupation numbers are defined as usual: $n_{\mathbf{k}}=[\exp(\beta\omega_{\mathbf{k}})-1]^{-1}$. The expression (2.5) reflects the contribution of Raman processes: a "spin wave" is scattered from $\mathbf{k}$ to $\mathbf{k}+\mathbf{q}$ with the same energy (actually differing by the electronic Zeeman energy $\hbar\omega_0$). We note that the second sum in the expressions for $S(\mathbf{q},\omega)$ given in Refs. 13 and 15, according to the creation or destruction of two bosons in the nuclear spin-relaxation process, vanishes at frequencies less than twice the excitation gap, so we have not included that sum here.

The preceding explicit calculation of T_1^{-1} proceeds most readily by first carrying out the integration over $\mathbf{q}$, which can be written in the form

$$\frac{\omega_{\mathbf{k}}}{(\lambda\eta)^2|\gamma_{\mathbf{k}}|}\int\frac{d^2p}{(2\pi)^2}A^2(\mathbf{p}-\mathbf{k})\left[\delta(\gamma_{\mathbf{p}}+\gamma_{\mathbf{k}})+\left[\frac{\omega_{\mathbf{k}}}{\lambda}\right]^2\delta(\gamma_{\mathbf{p}}-\gamma_{\mathbf{k}})\right]\ . \tag{2.8}$$

The prefactor here is $|d\omega_{\mathbf{k}}/d\gamma_{\mathbf{k}}|^{-1}$; it arises from changing the argument of the δ-function in going from Eq. (2.5) to (2.8). In the CuO_2 planes with which we are concerned, the hyperfine components, for either the copper or oxygen sites, are[21] of the general form

$$\sum_{\nu} A_{\nu}^2(\mathbf{q}) = A_0 + A_1\gamma_{\mathbf{q}} + A_2\gamma_{\mathbf{q}}^2 .$$

Since the delta functions within the integral in Eq. (2.8) exhibit the full fourfold rotational symmetry of the reciprocal lattice, we can replace $A^2(\mathbf{p}-\mathbf{k})$ there by its average over the four rotationally equivalent values of $\mathbf{p}$, which allows for the factorizations within the integrand:

$$\begin{aligned} &\gamma_{\mathbf{p}-\mathbf{k}} \to \gamma_{\mathbf{k}}\gamma_{\mathbf{p}} , \\ &4\gamma_{\mathbf{p}-\mathbf{k}}^2 \to 1 + \gamma_{2\mathbf{k}}\gamma_{2\mathbf{p}} + \cos k_x \cos k_y \cos p_x \cos p_y . \end{aligned} \tag{2.9}$$

Then if we use the standard integral representation of the delta function,

$$2\pi\delta(x) = \int ds \exp(ixs) ,$$

the two-dimensional integration over $\mathbf{p}$ gives the sum of products of two Bessel functions of integral order and argument $s/2$. The remaining integration over s is a Fourier transform of these functions, which is readily expressed in terms of complete elliptic integrals.

For example, with the simplest, constant, form factor $A^2(\mathbf{q}) = A^2$, we find

$$\frac{1}{T_1} = \frac{2A^2}{3\pi\eta^2} \int \frac{d^2k}{(2\pi)^2} \frac{e^{\beta\omega_{\mathbf{k}}}}{(e^{\beta\omega_{\mathbf{k}}}-1)^2} \times \frac{K[(1-\gamma_{\mathbf{k}}^2)^{1/2}]}{\omega_{\mathbf{k}}|\gamma_{\mathbf{k}}|} \left[1 + \left[\frac{\omega_{\mathbf{k}}}{\lambda}\right]^2\right] . \tag{2.10}$$

Since the integrand depends on $\mathbf{k}$ only through the combination of $\gamma_{\mathbf{k}}$, we can use the transformation

$$d^2k \to 8K[(1-\gamma_{\mathbf{k}}^2)^{1/2}]d\gamma_k ,$$

and integrate over $-1 \le \gamma_{\mathbf{k}} \le 1$. The logarithmic singularity from $\gamma_{\mathbf{k}}$ near zero is cut off by the finite resonance frequency. The contribution to T_1^{-1} from this region of the integral is of order

$$(A^2/J)\exp(-J/T)\ln^3(J/\omega_0) ,$$

which is small compared to the contributions from the region $\gamma_{\mathbf{k}}^2$ near unity. Here the excitation energy is small compared to the temperature, and the Bose factor $\exp(\beta\omega_{\mathbf{k}})-1$ can be replaced by $\beta\omega_{\mathbf{k}}$. Moreover, the final factor $(1+\omega_{\mathbf{k}}^2/\lambda^2)$ in Eq. (2.10) can be replaced by unity. The corresponding dominant contribution to T_1^{-1} takes the form

$$\frac{1}{T_1} \approx \frac{8A^2T^2K^2(0)}{3\pi^3J^3} \int^1 \frac{d_\gamma}{(1-\eta^2\gamma^2)^{3/2}} \approx \frac{8A^2T^2\xi}{3\pi J^3} , \tag{2.11}$$

where we have used Eq. (2.7) to write the answer in terms of the spin-correlation length ξ.

In calculating this dominant contribution to the relaxation rate (which, with suitable interpretation of the constant A^2, is appropriate to the Cu nuclei), it is allowable to replace $\gamma_{\mathbf{k}}^2$ by unity in all terms of the integrand in Eq. (2.10) except for the rapidly varying denominator $\omega_{\mathbf{k}}^3$. For the more general case,

$$A^2(\mathbf{q}) = A_0 + A_1\gamma_{\mathbf{q}} + A_2\gamma_{\mathbf{q}}^2 ,$$

we must replace $A^2(1+\omega_{\mathbf{k}}^2/\lambda^2)$ in Eq. (2.10) by

$$(A_0 - A_1 + A_2) + (A_0 + A_1 + A_2)(\omega_{\mathbf{k}}^2/\lambda^2) ,$$

and

$$K[(1-\gamma_{\mathbf{k}}^2)^{1/2}] \approx K(0) = \pi/2 ;$$

$$E[(1-\gamma_{\mathbf{k}}^2)^{1/2}] \approx E(0) = \pi/2$$

(see Appendix A). This simply leads to the replacement of A^2 in Eq. (2.11) by $A_0 - A_1 + A_2$ (so long as this does not vanish, as it does by symmetry at the oxygen site; see the following). The temperature dependence $T^2\xi(T)$ is to be compared with similar results of other approximations: Using the spherical approximation for the static electron spin correlations and an estimate of the relevant dynamics from the second frequency moment of the dynamic susceptibility, a method equivalent to the Onsager reaction field approach,[22] Shastry[12] finds $T_1^{-1} \sim T\xi$ with $\xi \approx 8e^{2J/T}$. Chakravarty and Orbach[17] use the dynamic structure factor generated earlier[10] by a combination of hydrodynamic, scaling, and renormalization analysis plus a fit to a classical rotor model, to obtain $T_1^{-1} \sim T^{3/2}\xi$ [with $\xi_C \approx 0.5e^{\alpha' J/T}(1+T/\alpha' J)^{-1}$ and $\alpha' \approx 0.94$]. This is the result based on the nonlinear σ model calculation of Chakravarty, Halperin, and Nelson[23] taken to two-loop order. Thus the results for the nuclear relaxation rate of the spherical model and the theory described in this section differ from the more sophisticated scaling approach only by slightly different numerical coefficients in the exponent and powers of T in the prefactor.[24] The preceding results also suggest that, at temperatures sufficiently high, $(J/T)^2e^{-2J/T}\ln^3(J/\omega_0)$ of order unity, we should expect to see a field dependence of the nuclear relaxation rate arising from spin fluctuations with energies $\omega_{\mathbf{k}} \sim J$ (where $\gamma_{\mathbf{k}} \approx 0$ and the joint density of states for Raman processes of vanishing energy transfer is high because of "nested" equal energy surfaces of the "spin waves"). Of course, this specific form of the result holds only if the temperature necessary to see the behavior is still sufficiently small for the low-temperature from of $S(\mathbf{q},\omega)$ which we have already used to remain valid.

For the oxygen nuclei, the hyperfine form factor due to neighboring Cu atoms is

$$\sum_{\nu} A_{\nu}^2(\mathbf{q}) = A^2(1+\gamma_{\mathbf{q}}) ,$$

which explicitly exhibits the vanishing of the hyperfine field due to fluctuations at the antiferromagnetic wave vector, as obviously must be the case by symmetry. It is these fluctuations which determine the dominant behavior of T_1^{-1} in Eq. (2.11). The extra factor of

$1+\gamma_q \rightarrow 1+\gamma_k\gamma_p$, when inserted in the integrand of Eq. (2.8), leads to the result

$$\frac{1}{T_1} \approx \frac{8A^2T^2K^2(0)}{3\pi^3J^3}\int_{1-T^2/8J^2}^{1} d\gamma \frac{1+\gamma^2+\eta^{-2}}{(1-\eta^2\gamma^2)^{1/2}} \approx \frac{A^2T^3}{2\pi J^4} . \tag{2.12}$$

The lower limit here has been set by the requirement $\beta\omega_k \lesssim 1$, where the Bose factor $\exp(\beta\omega_k)-1 \approx \beta\omega_k$; contributions from smaller γ_k are reduced effectively by factors of order $e^{-J/T}$ coming from the occupation number factor n_k which requires the presence of a spin wave of the corresponding energy for the Raman scattering process to take place. Just as for the Cu nuclei, there is also a field-dependent contribution from the region $\gamma_k \approx 0$, of the same functional form as predicted above. Also as before, the behavior of Eq. (2.12) can be compared with the corresponding result in Ref. 12, where Shastry finds $T_1^{-1} \sim T$.

Returning to the Cu site, we examine the Mila-Rice[21] hyperfine Hamiltonian for Cu. In order to explain the anisotropies observed in the Knight shift tensor and the relaxation rate for Cu in $YBa_2Cu_3O_7$, Mila and Rice proposed the following Hamiltonian:

$$H_{hf} = \sum_{\alpha} A^{\alpha\alpha} I_i^{\alpha} S_i^{\alpha} + \sum_{\delta} B \mathbf{I}_i \cdot \mathbf{S}_{i+\delta} . \tag{2.13}$$

Here $A^{\alpha\alpha}$ is an anisotropic on-site hyperfine coupling and B is an anisotropic transferred hyperfine coupling to nearest-neighbor Cu^{2+} spins. Normalizing with respect to the largest coupling $|A^{zz}|$, the hyperfine form factors for fields in the a-b plane and parallel to the c axis are

$$F_{ab}(\mathbf{q}) = \left[\frac{1-a^{xx}}{2} - 4b\gamma_q\right]^2 + \left[\frac{1+a^{xx}}{2}\right]^2 , \tag{2.14a}$$

$$F_c(\mathbf{q}) = (a^{xx}+4b\gamma_q)^2 , \tag{2.14b}$$

with $a^{xx} = A^{xx}/|A^{zz}|$, $b = B/|A^{zz}|$, and $\gamma_q = \frac{1}{2}(\cos q_x + \cos q_y)$. With the values of $a^{xx} \approx 0.02$ and $b \approx 0.18$ proposed by Mila and Rice for the CuO_2 lattice we find the ratio $(T_1^{-1})_{ab}/(T_1^{-1})_c$ to be approximately 3.5 at low temperatures.

Figure 1 shows numerical results for T_1^{-1} for the insulating case. Here the solid curve is for an on-site Cu form factor $A(\mathbf{q})=1$ and the dashed line is for an O nearest-neighbor Cu form factor $A^2(1+\gamma_q)$. If the effect of additional doped holes were simply to cut off the low-temperature divergence of ξ at some length l, one could write

$$\xi_{\text{eff}}^{-1} = \xi^{-1} + l^{-1} . \tag{2.15}$$

Using ξ_{eff} in Eq. (2.7) to determine η, results for T_1^{-1} with $l \approx 100$ are shown in Fig. 2. In the region around $T \sim 0.25$, the solid line exhibits some of the qualitative features of the experimentally observed T_1^{-1} Cu relaxation. However, the O relaxation continues to vary as T^3. In addition, the experimental cut-off length l seems to be only a few lattice spacings, which is much smaller than the value we used.

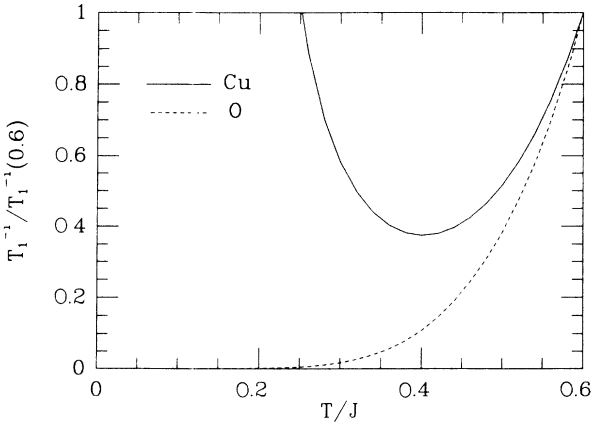

FIG. 1. Nuclear relaxation rate T_1^{-1}, scaled by its value at $T/J=0.6$, for the Cu and O sites in the insulating state.

The Knight shifts at both the Cu and O nuclei are also readily given within the theoretical framework being used here. By definition we have

$$K_i = \frac{1}{2}\left[\frac{\gamma_e}{\gamma_n}\right] A_i(\mathbf{q}=0)\chi_{vv}(\mathbf{q}=0) , \tag{2.16}$$

in units of γ_e/γ_n, where γ_e and γ_n are the electronic and appropriate ($\gamma_n = \gamma_{ni}$ depends on the nucleus but we will drop the i) nuclear gyromagnetic ratios, respectively, and the subscript i refers to either the Cu or the O nuclei,

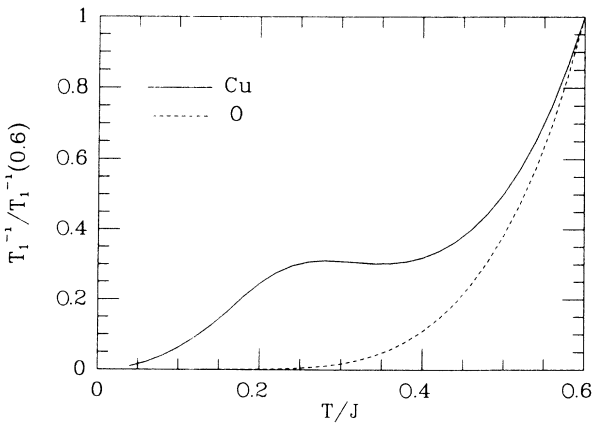

FIG. 2. Nuclear relaxation rate T_1^{-1}, scaled by its value at $T/J=0.6$, for the Cu and O sites in the strong-coupling regime with a finite cut off ($l \approx 100$) for the correlation length.

with their individual hyperfine coupling factors $A_i(\mathbf{q}=0)$. The low temperature limit[25] of the susceptibility is given[13,14] within spin-wave calculations as $\chi_{vv}(\mathbf{q}=0) \sim C/12J$, with $C \sim 0.5$.

III. THE 2D HUBBARD MODEL

In order to treat doped systems with metallic behavior, we now consider the 2D Hubbard model on a square lattice,

$$H=-t\sum_{\langle ij\rangle\sigma}(c_{i\sigma}^{\dagger}c_{j\sigma}+c_{j\sigma}^{\dagger}c_{i\sigma})+U\sum_{i}n_{i\uparrow}n_{i\downarrow}\ . \tag{3.1}$$

Here t is the one-electron nearest-neighbor overlap matrix element, corresponding to a bandwidth $W=8t$; and U is the on-site Coulomb interaction. In the following, we measure energies in units of t (or, when specified, in units of the bandwidth W) and continue to set $\hbar=k_B=1$.

The dynamic susceptibility $\chi(\mathbf{q},\omega)$ which determines K and T_1^{-1}, can be calculated from the finite-temperature Green's function

$$\chi(\mathbf{q},\tau)=\langle T_\tau[M_{\mathbf{q}}^{+}(\tau)M_{\mathbf{q}}^{-}(0)]\rangle\ , \tag{3.2}$$

where

$$M_{\mathbf{q}}^{+}=\frac{1}{\sqrt{N}}\sum_{\mathbf{p}}c_{\mathbf{p}+\mathbf{q}\uparrow}^{\dagger}c_{\mathbf{p}\downarrow} \tag{3.3}$$

and T_τ is the usual τ-ordering operator. Analytic continuation of the Matsubara Fourier transform $\chi(\mathbf{q},i\omega_m\rightarrow\omega+i0^+)$ yields $\chi(\mathbf{q},\omega)$. For a local contact hyperfine coupling $A\mathbf{I}_i\cdot\mathbf{S}_i$, the Knight shift K is given by

$$K=\frac{1}{2}\left[\frac{\gamma_e}{\gamma_n}\right]A\chi(\mathbf{q}\rightarrow 0,\omega=0) \tag{3.4}$$

and T_1^{-1} is given by

$$T_1^{-1}=\frac{T}{N}\sum_{\mathbf{q}}A^2\frac{\mathrm{Im}\chi(\mathbf{q},\omega_0)}{\omega_0}\ . \tag{3.5}$$

As before, ω_0 is the electronic Zeeman frequency, which can be set to zero on the scale of the energies of interest.

On a 2D square lattice the band energy is

$$\varepsilon_{\mathbf{k}}=-2(\cos k_x+\cos k_y)\ ,$$

and the single-particle density of states is

$$N(\varepsilon)=\frac{1}{N}\sum_{\mathbf{k}}\delta(\varepsilon-\varepsilon_{\mathbf{k}})=\frac{1}{2\pi^2}\mathbf{K}[(1-(\varepsilon/4)^2)^{1/2}]\ , \tag{3.6}$$

with $\mathbf{K}$ the complete elliptic integral. $N(\varepsilon)$ is plotted in Fig. 3, and shows the well-known logarithmic Van Hove singularity at $\varepsilon=0$. For a noninteracting system with $U=0$, the magnetic susceptibility takes the form

$$\chi_0(\mathbf{q},\omega)=\frac{1}{N}\sum_{\mathbf{p}}\frac{f(\varepsilon_{\mathbf{p}+\mathbf{q}})-f(\varepsilon_{\mathbf{p}})}{\omega-(\varepsilon_{\mathbf{p}+\mathbf{q}}-\varepsilon_{\mathbf{p}})+i0^+} \tag{3.7}$$

with

$$f(\varepsilon_{\mathbf{p}})=1/(\varepsilon^{\beta(\varepsilon_{\mathbf{p}}-\mu)}+1)$$

the Fermi function and μ the chemical potential, which is zero for a half-filled band. Thus, for $U=0$ we have

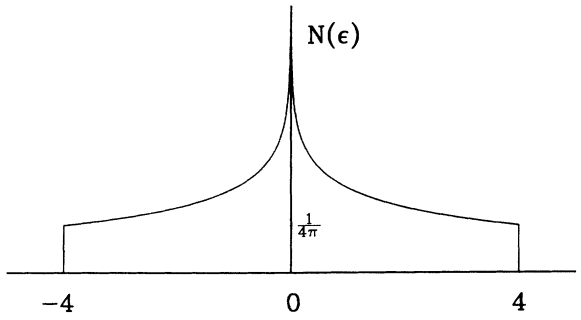

FIG. 3. Density of states $N(\varepsilon)$ for the noninteracting 2D Hubbard model.

$$K=\frac{1}{2}\left[\frac{\gamma_e}{\gamma_n}\right]A\beta\int_{-\infty}^{\infty}d\varepsilon\,N(\varepsilon)f(\varepsilon)[1-f(\varepsilon)] \tag{3.8}$$

and

$$\frac{1}{T_1}=\pi A^2\int_{-\infty}^{\infty}d\varepsilon\,N^2(\varepsilon)f(\varepsilon)[1-f(\varepsilon)]\ , \tag{3.9}$$

with $N(\varepsilon)$ given by Eq. (3.6). At low temperatures

$$K=\tfrac{1}{2}(\gamma_e/\gamma_n)AN(\mu)$$

and

$$T_1^{-1}=\pi A^2N^2(\mu)T\ ,$$

so that $(T_1TK^2)^{-1}$, measured in units of $4\pi\gamma_n^2/\gamma_e^2$, is unity:

$$(T_1TK^2)^{-1}=1\ . \tag{3.10}$$

This is the well-known Korringa relation for a free electron gas where T_1^{-1} varies linearly with temperature. At higher temperatures the full integrals in Eqs. (3.8) and (3.9) give the temperature dependence for K, T_1^{-1}, and $(T_1TK^2)^{-1}$ as shown by the dashed curves in Fig. 4(a)–(c) for a hole filling of $n_h=1.135$ per site. The Van Hove singularity in $N(\varepsilon)$ at $\varepsilon=0$ causes $(T_1T)^{-1}$ and K to exhibit finite-temperature peaks for fillings away from $n_h=1$.

For the interacting system, we approximate $\chi(\mathbf{q},\omega)$ using the RPA expression,

$$\chi(\mathbf{q},\omega)=\frac{\chi_0(\mathbf{q},\omega)}{1-U\chi_0(\mathbf{q},\omega)}\ . \tag{3.11}$$

This approximation is known to give an unphysical phase transition for the 2D Hubbard model when $U\chi_0(\mathbf{q}^*,0)=1$. In Fig. 5, we show the phase diagram obtained within the RPA (Ref. 26) for $U/W=0.25$. We assume above a hole filling of $n_h=1.135$. This choice places the model in a paramagnetic metallic regime with significant antiferromagnetic fluctuations for $T\rightarrow 0$. Note that our treatment is necessarily phenomenological: An RPA analysis is not sufficient to reproduce the de-

tailed functional dependences of K and T_1^{-1} on U and the band filling. However, if U and n_h are chosen appropriately, such an analysis does incorporate the essential features of large-q spin fluctuations.

Substituting the RPA expression (3.11) for $\chi(\mathbf{q},\omega)$ in Eqs. (3.4) and (3.5), we have evaluated K and T_1^{-1} for an on-site contact hyperfine coupling. The results for K, T_1^{-1}, and $(T_1TK^2)^{-1}$ are shown as the solid curves in Figs. 4(a)–4(c). For the parameters chosen, the RPA Knight shift is enhanced by approximately a Stoner factor of 2 over the result for $U=0$. Because of the important influence of strong antiferromagnetic fluctuations on T_1^{-1}, the latter is enhanced much more—over a factor of 10—at low temperatures. While at low temperatures T_1^{-1} eventually tends to zero linearly (since the RPA ground state is paramagnetic), it deviates from linear behavior at higher temperatures, becoming nearly flat. Note that the Korringa ratio is also enhanced by the large-q fluctuations in $\chi(\mathbf{q},\omega)$, which enter T_1^{-1}, but not K.[27]

As we have seen, for an *on-site* hyperfine coupling, large-momentum spin fluctuations enhance T_1^{-1}. More generally, for a nonlocal hyperfine interaction, a form factor enters the calculation of T_1^{-1} and filters the spin

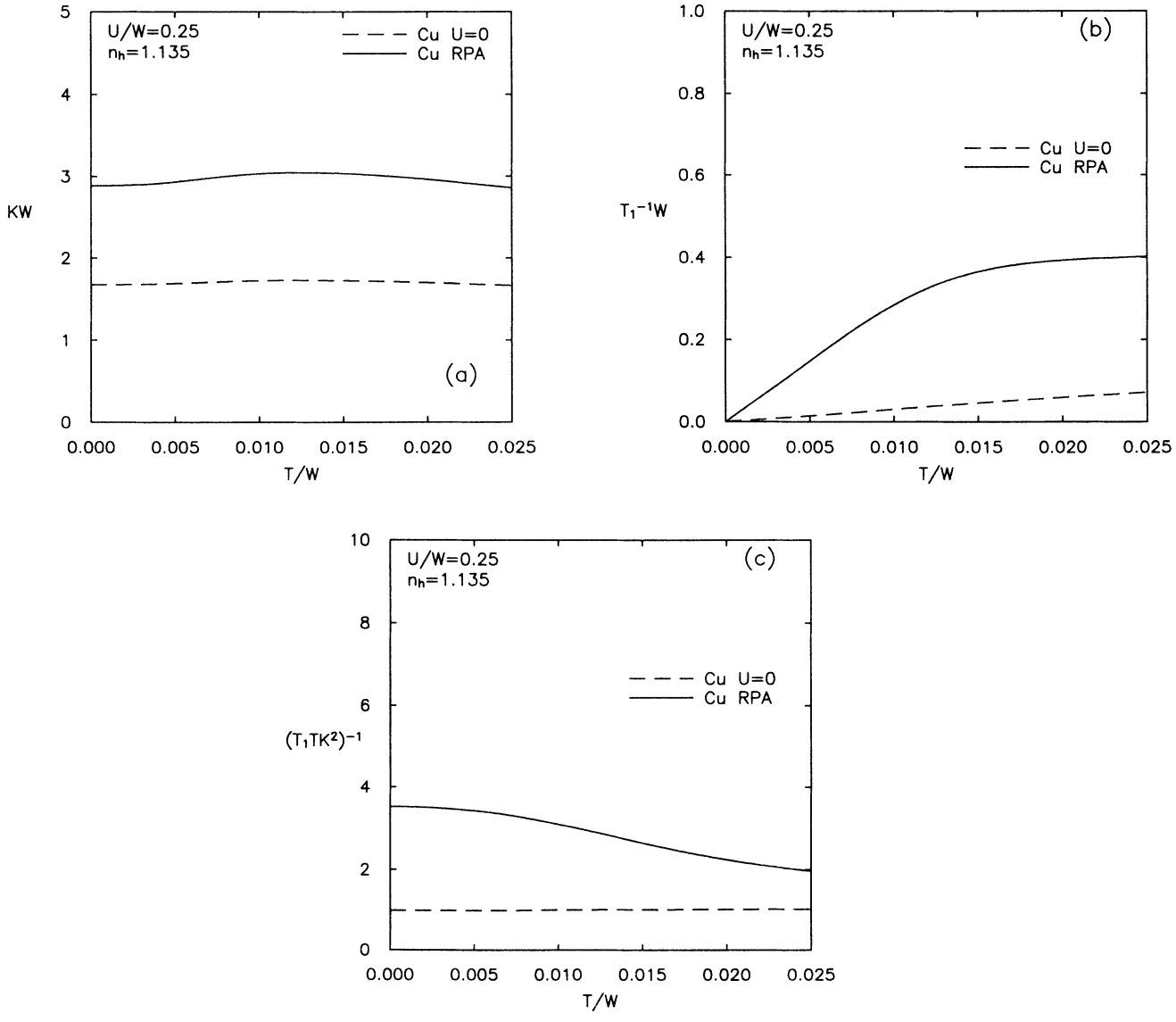

FIG. 4. Cu NMR for isotropic on-site hyperfine coupling in the Hubbard model. (a) Knight shift K, in units of $\frac{1}{2}(\gamma_e/\gamma_n)A$. (b) Nuclear relaxation rate T_1^{-1}, in units of πA^2. (c) Korringa ratio $(T_1TK^2)^{-1}$, in units of $4\pi\gamma_n^2/\gamma_e^2$. Energies are measured in units of the bandwidth $W=8t$. The hole filling is chosen to place the system on the paramagnetic edge of the RPA instability for $T\rightarrow 0$. Results are shown for the noninteracting system and for $U/W=0.25$ within RPA.

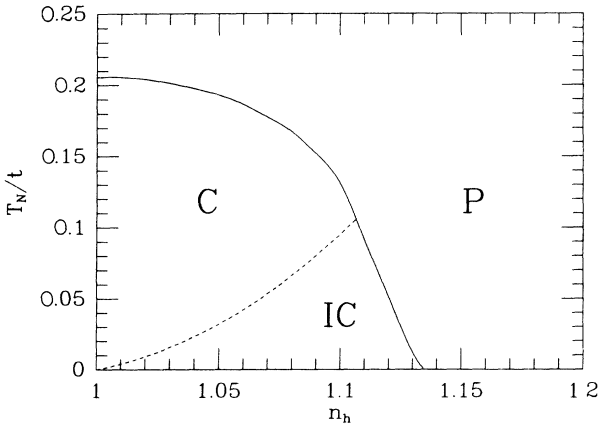

FIG. 5. The phase diagram of the 2D Hubbard model within RPA (Ref. 26) for $U/W=0.25$. The three phases are as follows: P=paramagnetic, C=commensurate, and IC=incommensurate spin-density wave.

fluctuations sampled by nuclei at different sites. For example, as discussed in Sec. II, if the planar O nuclear spin has an isotropic hyperfine coupling to the two nearest-neighbor Cu spins

$$H_{\rm hf}=A\mathbf{I}_O\cdot(\mathbf{S}_1+\mathbf{S}_2)\ , \tag{3.12}$$

then the relaxation rate for O nuclei is

$$T_1^{-1}=TA^2\lim_{\omega\to 0}\frac{1}{N}\sum_{\mathbf{q}}F_2(\mathbf{q})\frac{{\rm Im}\chi(\mathbf{q},\omega)}{\omega}\ ,$$
$$F_2(\mathbf{q})=4\cos^2(q_\alpha/2)\ . \tag{3.13}$$

Here $\alpha=x$ or y according to whether the O nuclei are on Cu—Cu bonds with x or y orientation. By symmetry, both choices give the same relaxation rate.

In this case the antiferromagnetic $\mathbf{q}^*=(\pi,\pi)$ fluctuations of the Cu moment cancel at the O site. The results for T_1^{-1} and $(T_1TK^2)^{-1}$ are plotted in Figs. 6(a)–6(b). Note the much smaller enhancement of the oxygen relaxation compared to that of Cu. While the temperature dependence of T_1^{-1} on the O site is clearly not completely Korringa-like, it is nearly linear with an enhanced slope over a wide temperature range. In Sec. IV, we will examine the scenario in which the oxygen form factor arises from coupling to nearest-neighbor O (rather than Cu) sites; in this case, the O relaxation clearly follows a Korringa behavior over the relevant temperature region.

In order to contrast the results for Cu and O NMR, it is useful to replot the relaxation rate and Korringa ratio in scaled forms. In Fig. 7(a), the Cu and O relaxation rates are scaled by their respective values at $T/W=0.025$. On this plot, it is possible to find a temperature window (which might span the experimental range from T_c up to room temperature) within which the O relaxation is essentially Korringa-like, while the Cu relaxation is nonlinear. Within this window, as seen in Fig. 7(b), the dimensionless enhancement of the Korringa ratio

$$(T_1TK^2)^{-1}/(T_1TK^2)_0^{-1}$$

increases sharply with decreasing temperature on the Cu sites, while remaining nearly temperature-independent on the O sites. An even larger enhancement for the Cu sites could be obtained by positioning n_h closer to the RPA magnetic phase boundary; as mentioned previously, this sensitivity to filling is a largely unphysical consequence of the RPA, and a more precise estimate of the Korringa enhancement is not possible within the current analysis. There have also been attempts[28] to fit T_1^{-1} experimental data for doped $YBa_2Cu_3O_7$ to a $T^{1/2}$ curve, following the work of Moriya and Ueda[29] in 3D. However, in 2D the

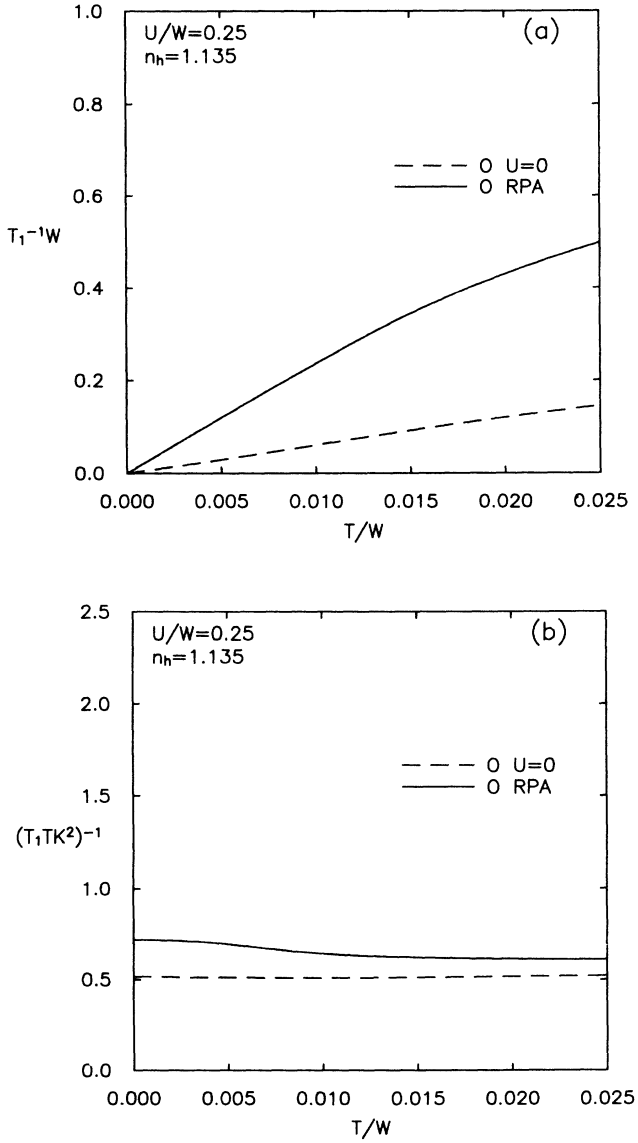

FIG. 6. O NMR for an isotropic transferred hyperfine coupling to nearest-neighbor Cu spins in the Hubbard model. (a) Nuclear relaxation rate T_1^{-1}, in units of πA^2. (b) Korringa ratio $(T_1TK^2)^{-1}$, in units of $4\pi\gamma_n^2/\gamma_e^2$.

phase space for antiferromagnetic fluctuations is reduced, giving a temperature dependence of $T_1^{-1} \approx T(T-T_N)^{-1}$ near $T=T_N$, rather than the Moriya-Ueda $T(T-T_N)^{-1/2}$ form. Thus for $T_N \to 0$, the low-temperature limit of the 2D result for T_1^{-1} approaches a constant rather than varying as $T^{1/2}$.

We conclude this section by considering the Mila-Rice transferred hyperfine coupling in the Hubbard model. Using the form factors given in Eq. (2.13), $(T_1^{-1})_{ab}$ and $(T_1^{-1})_c$ for Cu sites are plotted in Fig. 8. Both functions resemble the result for an isotropic hyperfine coupling in Fig. 4. The anisotropy ratio $(T_1^{-1})_{ab}/(T_1^{-1})_c$ is nearly temperature independent and approximately equal to 3.8 throughout the range shown.

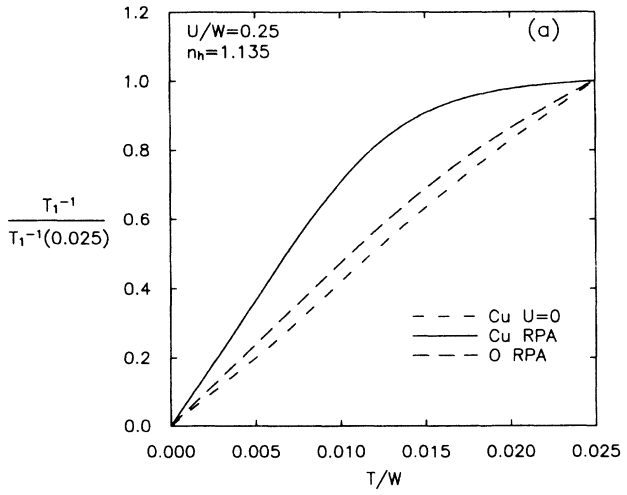

FIG. 7. Comparisons with Korringa behavior for NMR in the Hubbard model. (a) Nuclear relaxation rate T_1^{-1}, scaled by its value at $T/W=0.025$. For strict Korringa behavior over this temperature interval, the plot would be a straight line. (b) Enhancement of the Korringa ratio $(T_1TK^2)^{-1}/(T_1TK^2)_0^{-1}$ within RPA.

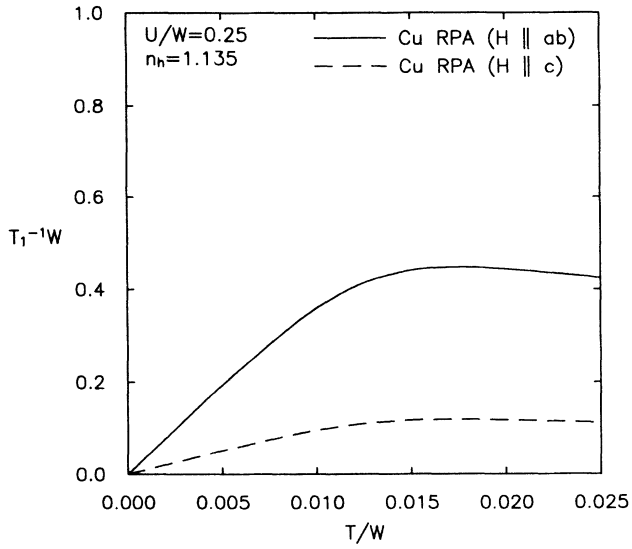

FIG. 8. Cu NMR for the anisotropic Mila-Rice relaxation mechanism in the Hubbard model. Nuclear relaxation rate T_1^{-1}, in units of $\pi(A^{zz})^2$. The assumed values of $a^{xx}=A^{xx}/|A^{zz}|$ and $b=B/|A^{zz}|$ are $4.7/222.7=0.02$ and $40.7/227.7=0.18$, respectively.

IV. THE 2D CuO_2 LATTICE

In this section, we consider a more detailed model for the CuO_2 layers in $YBa_2Cu_3O_{7-x}$. We assume that holes occupy strongly hybridized

$$\mathrm{Cu}(3d_{x^2-y^2})-\mathrm{O}(2p\sigma)$$

orbitals and that the Coulomb repulsion between $3d$ holes is the dominant many-body effect. The unit cell (Fig. 9) has a three-orbital basis. The resulting Hamiltonian takes the form

$$\begin{aligned} H-\mu N_h &= H_{\mathrm{site}}+H_{\mathrm{hop}}+H_{\mathrm{Coul}}-\mu N_h \ , \\ H_{\mathrm{site}} &= \varepsilon \sum_{i\sigma}(n_{ia\sigma}+n_{ib\sigma}) \ , \\ H_{\mathrm{hop}} &= -t\sum_{i\sigma}[d_{i\sigma}^{\dagger}(a_{i\sigma}+a_{i-x\sigma})+\mathrm{H.c.}] \\ &\quad -t\sum_{i\sigma}[d_{i\sigma}^{\dagger}(b_{i\sigma}+b_{i-y\sigma})+\mathrm{H.c.}] \ , \qquad (4.1) \\ H_{\mathrm{Coul}} &= U\sum_i n_{id\uparrow}n_{id\downarrow} \ , \\ N_h &= \sum_{i\sigma}(n_{id\sigma}+N_{ia\sigma}+n_{ib\sigma}) \ , \end{aligned}$$

where $d_{i\sigma}^{\dagger}$ creates a Cu($3d$) hole; $a_{i\sigma}^{\dagger}$ and $b_{i\sigma}^{\dagger}$ create O($2p\sigma$) holes; and $n_{i(dab)\sigma}$ are the corresponding number operators. Energies are measured relative to the Cu($3d$) level $\varepsilon_d=0$. For simplicity, the orbital phases are chosen to give all hopping integrals the same sign.

Writing

$$d_{i\sigma}=\frac{1}{\sqrt{N}}\sum_{\mathbf{k}} e^{i\mathbf{k}\cdot\mathbf{R}_i}d_{\mathbf{k}\sigma}$$

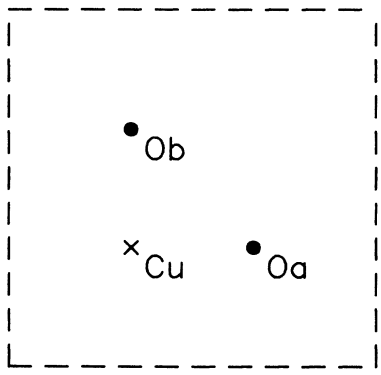

FIG. 9. Schematic three-site unit cell for the CuO_2 lattice.

with N the number of unit cells, and likewise for the oxygen orbitals, we find that the Hamiltonian reduces to a form convenient for calculations:

$$\begin{aligned} H-\mu N_h &= H_{\text{site}}+H_{\text{hop}}+H_{\text{Coul}}-\mu N_h \ , \\ H_{\text{site}} &= \varepsilon \sum_{\mathbf{k}\sigma} (a^{\dagger}_{\mathbf{k}\sigma}a_{\mathbf{k}\sigma}+b^{\dagger}_{\mathbf{k}\sigma}b_{\mathbf{k}\sigma}) \ , \\ H_{\text{hop}} &= -\sum_{\mathbf{k}\sigma} t_x(\mathbf{k})(d^{\dagger}_{\mathbf{k}\sigma}a_{\mathbf{k}\sigma}+\text{h.c.}) \\ &\quad -\sum_{\mathbf{k}\sigma} t_y(\mathbf{k})(d^{\dagger}_{\mathbf{k}\sigma}b_{\mathbf{k}\sigma}+\text{h.c.}) \ , \end{aligned} \tag{4.2a}$$

where

$$\begin{aligned} t_x &= 2t\cos(k_x/2) \ , \\ t_y &= 2t\cos(k_y/2) \ . \end{aligned} \tag{4.2b}$$

In the absence of Coulomb interactions, the spectrum consists of bonding and antibonding $\text{Cu}(3d)-\text{O}(2p\sigma)$ bands

$$E^{\pm}_{\mathbf{k}} = \tfrac{1}{2}\varepsilon \pm [(\tfrac{1}{2}\varepsilon)^2+t_x^2(\mathbf{k})+t_y^2(\mathbf{k})]^{1/2} \tag{4.3a}$$

and a nonbonding oxygen band

$$E^0_{\mathbf{k}} = \varepsilon \ . \tag{4.3b}$$

The hyperfine Hamiltonian which determines the Knight shift measured at a particular nuclear site takes the general form

$$H_{\text{hf}} = AI^z_{\text{i}} \sum_{\delta} S^z_{\text{i}+\delta,r} \ , \tag{4.4}$$

where A is a hyperfine coupling constant, I^z_{i} is the nuclear spin, and the $S^z_{\text{i}+\delta,r}$ are electronic spins at nearby sites of type r ($r=d,a,b$). In the simplest case, the coupling is on-site, i.e., $\delta=0$. The Knight shift is proportional to the electronic spin induced on site r by a magnetic field H. For example, for on-site coupling to the $\text{Cu}(3d)$ spin,

$$\begin{aligned} K_d &= \left[\frac{A}{\gamma_n H}\right]\langle S^z_{\text{id}}\rangle = \left[\frac{A}{\gamma_n H}\right]\tfrac{1}{2}\langle M^z_{\text{id}}\rangle \ , \\ &= \tfrac{1}{4}(\gamma_e/\gamma_n)A\int_0^{\beta}\Big\langle T_{\tau}\sum_{\text{j}}[M^z_{\text{jd}}(\tau)+M^z_{\text{ja}}(\tau) \\ &\qquad +M^z_{\text{jb}}(\tau)]M^z_{\text{id}}(0)\Big\rangle \ , \end{aligned} \tag{4.5a}$$

where

$$M^z_{\text{id}} = n_{\text{id}\uparrow}-n_{\text{id}\downarrow} \tag{4.5b}$$

and γ_n and γ_e are the nuclear and electronic gyromagnetic ratios. Summing the right-hand side of Eq. (4.5a) on i and dividing by the number of unit cells gives a simple expression in terms of partial susceptibilities:

$$\begin{aligned} K_r &= \tfrac{1}{2}(\gamma_e/\gamma_n)A\chi_r(\mathbf{q}\to 0,\omega=0) \ , \\ \chi_r(\mathbf{q},i\omega_m) &= \sum_{r=d,a,b}\chi_{r'r}(\mathbf{q},i\omega_m) \ , \\ \chi_{r'r}(\mathbf{q},i\omega_m) &= \int_0^{\beta}d\tau\, e^{i\omega_m\tau}\tfrac{1}{2}\langle T_{\tau}[M^z_{\mathbf{q}r'}(\tau)M^z_{-\mathbf{q}r}(0)]\rangle \ , \\ M_{\mathbf{q}r}(\tau) &= \frac{1}{\sqrt{N}}\sum_{\text{i}} e^{i\mathbf{q}\cdot\mathbf{R}_{\text{i}}}M_{\text{ir}}(\tau) \ . \end{aligned} \tag{4.6}$$

In the absence of interactions ($U=0$), the partial susceptibilities $\chi^0_{r'r}$ may be calculated exactly by transforming to the energy-band basis:

$$\begin{aligned} \chi^0_{r'r}(\mathbf{q},i\omega_m) &= \frac{1}{N}\sum_{\mathbf{k};\nu\nu'=0,\pm}\alpha^{\nu}_{r'r}(\mathbf{k}+\mathbf{q})\alpha^{\nu'}_{r'r}(\mathbf{k}) \\ &\quad \times\frac{f(E^{\nu}_{\mathbf{k}+\mathbf{q}})-f(E^{\nu'}_{\mathbf{k}})}{i\omega_m-(E^{\nu}_{\mathbf{k}+\mathbf{q}}-E^{\nu'}_{\mathbf{k}})} \ . \end{aligned} \tag{4.7}$$

The transformation factors $\alpha^{\nu}_{r'r}(\mathbf{k})$ are written out explicitly in Appendix A. Note that $\chi^0_{r'r}$ contains both intraband and interband contributions. Note also that since

$$\alpha^{\nu}_{rr'}(\mathbf{k}) = \alpha^{\nu}_{r'r}(\mathbf{k}) \ , \tag{4.8a}$$

it follows immediately that

$$\chi^0_{rr'}(\mathbf{q},i\omega_m) = \chi^0_{r'r}(\mathbf{q},i\omega_m) \ . \tag{4.8b}$$

In the presence of interactions, the Knight shifts are modified by the replacement $\chi^0_{r'r}\to\chi_{r'r}$. Within the random-phase approximation, the partial susceptibilities assume a particularly simple form when only an on-site Cu interaction is present. The neglect of on-site O and intersite Cu-O interactions may be called questionable, but it provides a plausible starting point for the description of *magnetic* phenomena. In this case,

$$\chi^{\text{RPA}}_{rr'} = \chi^0_{rr'}+\chi^0_{rd}\frac{U}{1-U\chi^0_{dd}}\chi^0_{dr'} \ . \tag{4.9}$$

The arguments of all functions are understood to be $(\mathbf{q},i\omega_m)$.

The nuclear spin-relaxation rates for the CuO_2 lattice are formally similar to those for the 2D Hubbard lattice. Assuming an isotropic on-site hyperfine coupling A between the electronic and nuclear spins of Cu, the Cu relaxation rate is just

$$(T_1^{-1})_{\mathrm{Cu}} = TA^2 \lim_{\omega\to 0} \frac{1}{N} \sum_{\mathbf{q}} \frac{\mathrm{Im}\chi_{dd}(\mathbf{q},\omega)}{\omega} \ . \tag{4.10}$$

The partial susceptibility χ_{dd} replaces the Hubbard susceptibility in Eq. (3.5). Likewise χ_{dd} replaces χ in Eq. (3.13), which applies (with different form factors F_{dd}) for (a) O nuclear relaxation by neighboring Cu spins; and (b) Cu nuclear relaxation by on-site and neighboring Cu spins (the Mila-Rice scenario).

Relaxation mechanisms based on O electronic spins may also be studied. In this case, a general expression for T_1^{-1}, assuming an isotropic coupling, is

$$T_1^{-1} = \frac{TA^2}{\pi N} \lim_{\omega\to 0} \sum_{\mathbf{q}} \left[F_{aa}(\mathbf{q}) \frac{\mathrm{Im}\chi_{aa}(\mathbf{q},\omega)}{\omega} + F_{ab}(\mathbf{q}) \frac{\mathrm{Im}\chi_{ab}(\mathbf{q},\omega)}{\omega} \right] . \tag{4.11}$$

To reach this form, we have combined contributions proportional to χ_{bb} and χ_{ba} with the first and second terms using symmetry considerations.

Assuming that O relaxation occurs by an isotropic transferred hyperfine coupling to the four neighboring O sites [e.g., through O(2s) admixture in the ground state] and neglecting on-site terms [see Fig. 10(a)], we find

$$F_{aa}(\mathbf{q}) = 4\left[\cos\left[\frac{q_x - q_y}{2}\right] + \cos\left[\frac{q_x + q_y}{2}\right]\right]^2 ,$$
$$F_{ab}(\mathbf{q}) = 0 \ . \tag{4.12a}$$

Finally, for relaxation of Y nuclei by neighboring O spins [four each in the layers above and below—see Fig. 10(b)],

$$F_{aa}(\mathbf{q}) = (2)8\cos^2(q_x/2) \ ,$$
$$F_{ab}(\mathbf{q}) = (2)8\cos(q_x/2)\cos(q_y/2) \ . \tag{4.12b}$$

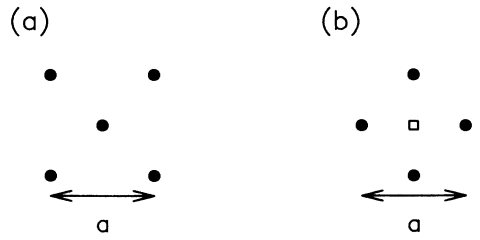

FIG. 10. Lattice sites involved in (a) transferred hyperfine coupling of O nuclei to nearest-neighbor O sites and (b) transferred hyperfine coupling of Y nuclei to nearest-neighbor O sites. Note that in the second case the relevant O sites lie in layers above and below the Y.

In this last case, it is assumed that spins in adjacent CuO_2 layers fluctuate independently, leading to the multiplicative factor of 2 in Eq. (4.12b).

The various form factor choices for relaxation by Cu and O spins are summarized in Table I. Note that if both types of relaxation are considered simultaneously, additional terms proportional to χ_{da} and χ_{db} enter the expressions for T_1^{-1} already given.

Results for the Cu Knight shift, relaxation rate, and Korringa ratio $(T_1 TK^2)^{-1}$, assuming an isotropic on-site relaxation process, are plotted in Figs. 11(a)–11(c). The assumed parameters are $\varepsilon = 0$, $n_h = 1.165$, and $U/W = 0.7$. As for the Hubbard model, the hole filling is chosen to place the system marginally on the paramagnetic side of the RPA phase boundary. Phenomenologically, this introduces strong antiferromagnetic fluctuations, while eliminating the finite-temperature phase transition predicted within RPA for fillings closer to unity. In order to emphasize similarities with the Hubbard results, it is convenient to measure energies (and temperatures) in

TABLE I. Form factors for hyperfine coupling Hamiltonians in the CuO_2 lattice. The first column lists the Nuclei where relaxation is to be measured; the second lists the source of relaxation (NN = nearest-neighbor); the third lists the symmetry of the hyperfine Hamiltonian under spin rotations; and the fourth lists the nonzero form factors.

Nucleus	Coupled to	Spin symmetry	Form factor
Cu	on-site Cu($3d$)	isotropic	$F_{dd} = 1$
	on-site Cu($3d$)	Mila-Rice	
		$\mathbf{H} \parallel a$-b	$F_{dd} = [\frac{1}{2}(1 - a^{xx}) - 4b\gamma_{\mathbf{q}}]^2 + \frac{1}{4}(1 + a^{xx})^2$
		$\mathbf{H} \parallel c$	$F_{dd} = (a^{xx} + 4b\gamma_{\mathbf{q}})^2$
O	NN Cu($3d$)	isotropic	$F_{dd} = 4\cos^2(q_x/2)$
	NN O($2p$)	isotropic	$F_{aa} = 4\left[\cos\left[\frac{q_x - q_y}{2}\right] + \cos\left[\frac{q_x + q_y}{2}\right]\right]^2$
Y	NN O($2p$)	isotropic	$F_{aa} = \cos^2(q_x/2)$, $F_{ab} = 16\cos(q_x/2)\cos(q_y/2)$

units of the bandwidth $W=2\sqrt{2}t$ of the lowest Cu-O band (note that for equal values of t, the Hubbard bandwidth is larger by a factor of $2\sqrt{2}$). As before, K and T_1^{-1} may be expressed in dimensionless units by scaling with W.

For the parameters chosen, the Knight shift exhibits an RPA enhancement of approximately 2 at low temperatures. As in the case of the Hubbard model, antiferromagnetic fluctuations enhance T_1^{-1} by more than an order of magnitude in the same temperature range. Further, T_1^{-1} deviates strongly from Korringa behavior at intermediate temperatures, becoming nearly flat over a significant temperature range. The presence of large-**q** fluctuations is also evident in the Korringa ratio, which is of order 3–4 at low temperatures. Note that due to band structure effects, the Korringa ratio of the noninteracting system is actually smaller than unity.

In Figs. 12(a) and 12(b), corresponding results are plotted for the oxygen relaxation rate and the Korringa ratio, assuming isotropic relaxation due to coupling with nearest-neighbor Cu spins. In this case, the form factor which enters T_1^{-1} has two important effects: (a) while the

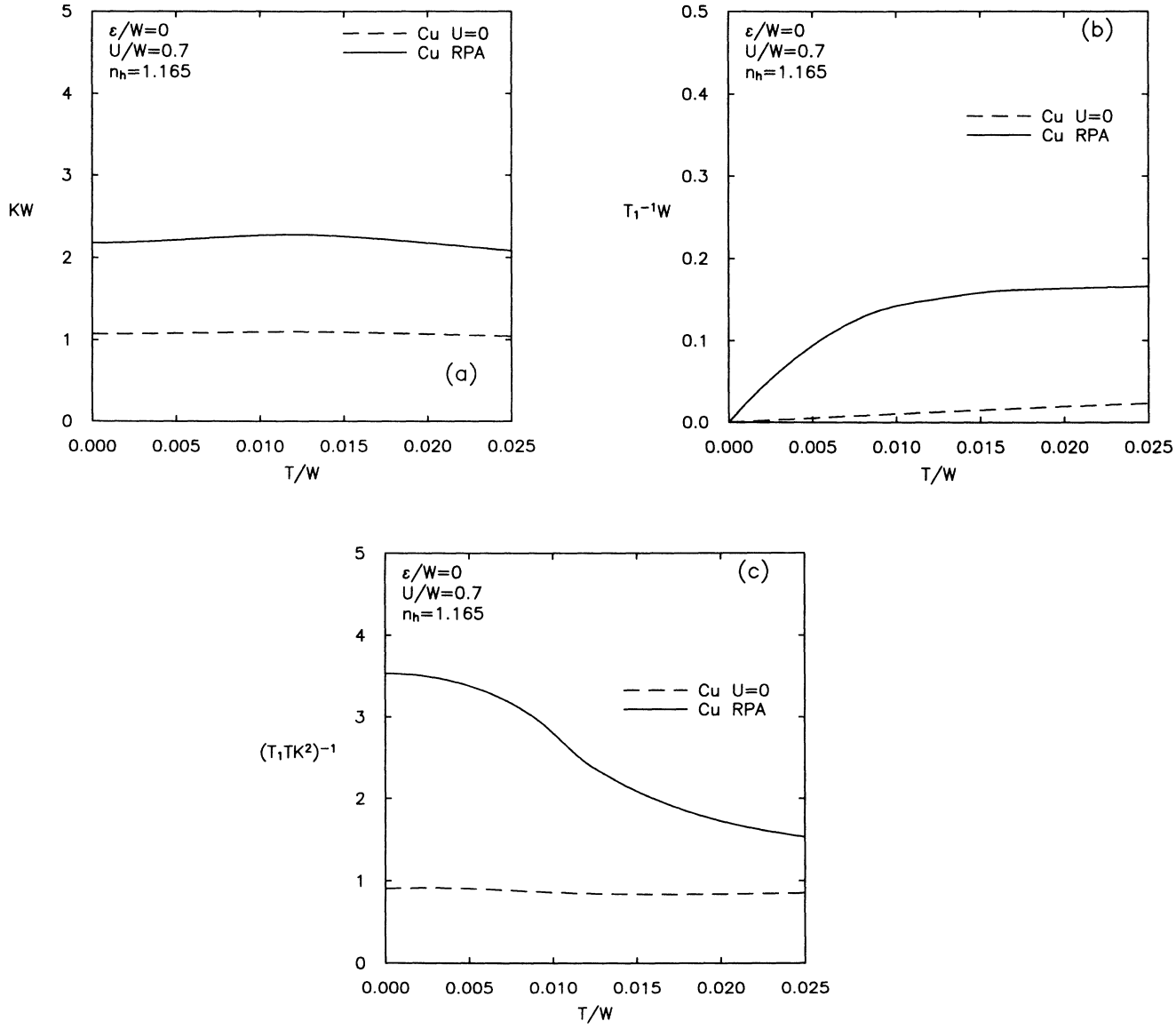

FIG. 11. Cu NMR for isotropic on-site hyperfine coupling in the CuO_2 model. (a) Knight shift K, in units of $\frac{1}{2}(\gamma_e/\gamma_n)A$. (b) Nuclear relaxation rate T_1^{-1}, in units of πA^2. (c) Korringa ratio $(T_1TK^2)^{-1}$, in units of $4\pi\gamma_n^2/\gamma_e^2$. Energies are measured in units of the width $w=2\sqrt{2}t$ of the lower ($E_{\mathbf{k}}^-$) Cu-O band. The Cu($3d$) and O($2p\sigma$) orbitals are assumed degenerate. The hole filling is chosen to place the system on the paramagnetic edge of the RPA instability for $T\rightarrow 0$. Results are shown for the noninteracting system and for $U/W=0.7$ within RPA.

Knight shift enhancement is the same as for Cu, T_1^{-1} is only enhanced about half as much as before; and (b) T_1^{-1} remains Korringa-like over a significantly larger temperature range.

As for the Hubbard model, it is useful to compare the temperature dependences of the Cu and O results directly. In Fig. 13(a), the RPA relaxation rates are replotted after scaling by their values at $T/W=0.025$ (which corresponds to room temperature for a bandwidth of 1 eV). As before, it is possible to find a window, corresponding to the range of experimentally accessible temperatures, throughout which the O relaxation is essentially Korringa-like, while the Cu relaxation exhibits strong deviations from linearity. Finally, the RPA enhancement of the Korringa ratio

$$(T_1TK^2)^{-1}/(T_1TK^2)_0^{-1},$$

which serves as a dimensionless measure of the strength of large-**q** fluctuations, is plotted in Fig. 13(b). This enhancement is of order 1.5 for the O sites, but more than twice as large for the Cu.

Results for T_1^{-1} within the more complex Mila-Rice scenario are shown in Fig. 14. The parameters assumed for this plot are as in Figs. 11–13. The coupling constant ratios a^{xx} and b are as in Fig. 8. As before, the ratio $(T_1)_{ab}^{-1}/(T_1)_c^{-1}$ is weakly temperature dependent and of order 4.2 throughout the range shown.

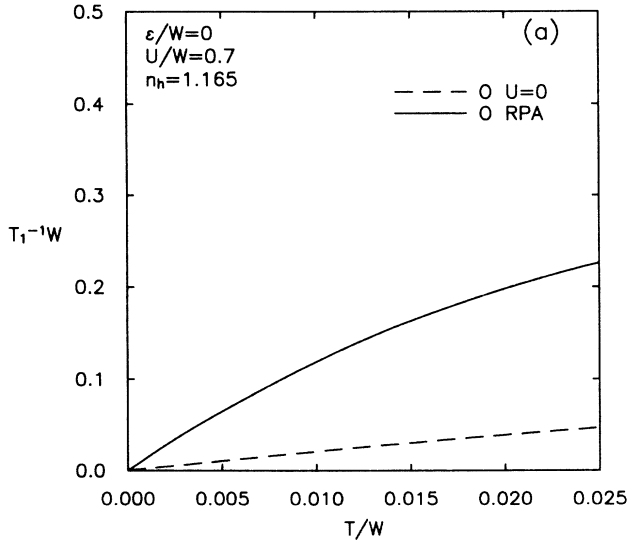

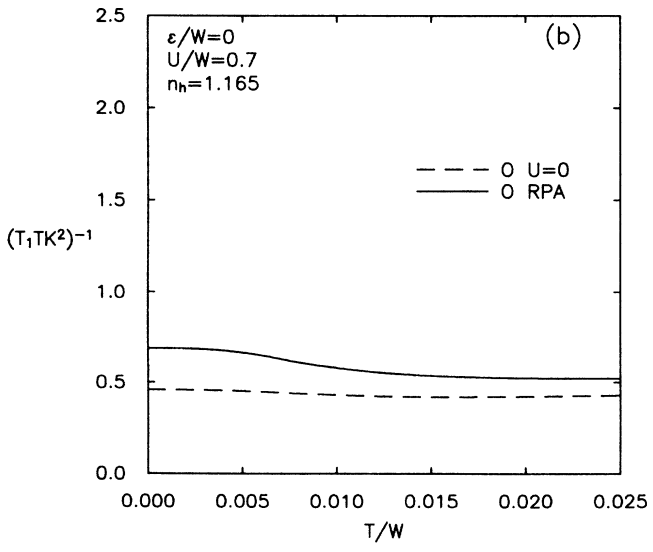

FIG. 12. O NMR for isotropic transferred hyperfine coupling to nearest-neighbor Cu spins in the CuO_2 model. (a) Nuclear relaxation rate T_1^{-1}, in units of πA^2. (b) Korringa ratio $(T_1TK^2)^{-1}$, in units of $4\pi\gamma_n^2/\gamma_e^2$.

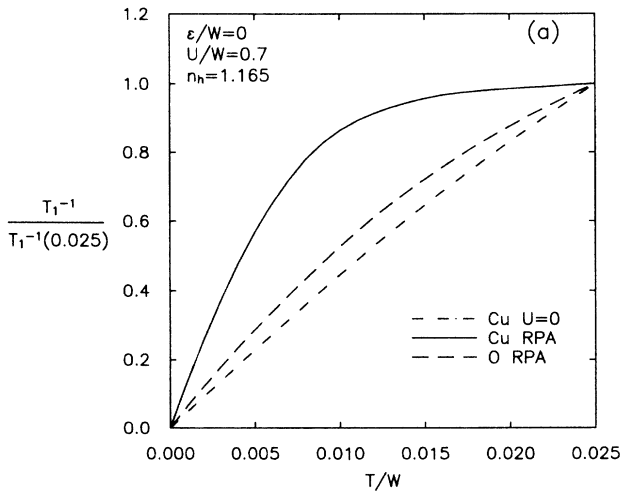

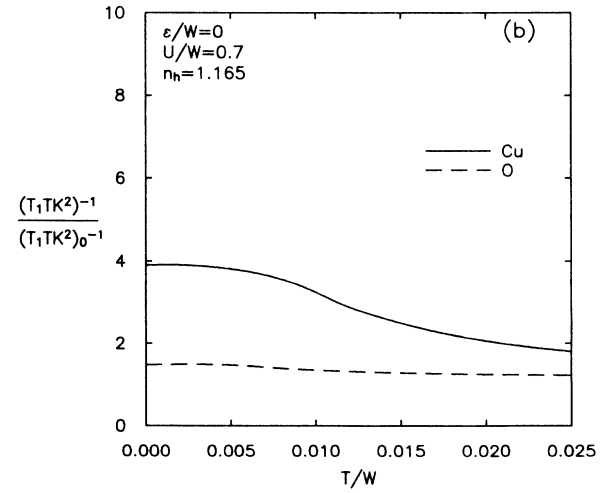

FIG. 13. Comparisons with Korringa behavior for NMR in the CuO_2 model. (a) Nuclear relaxation rate T_1^{-1}, scaled by its value at $T/W=0.025$. For strict Korringa behavior, the plot would be a straight line. (b) RPA enhancement of the Korringa ratio $(T_1TK^2)^{-1}/(T_1TK^2)_0^{-1}$, assuming an isotropic Cu(3d) relaxation mechanism for both Cu and O sites, as in Figs. 11 and 12.

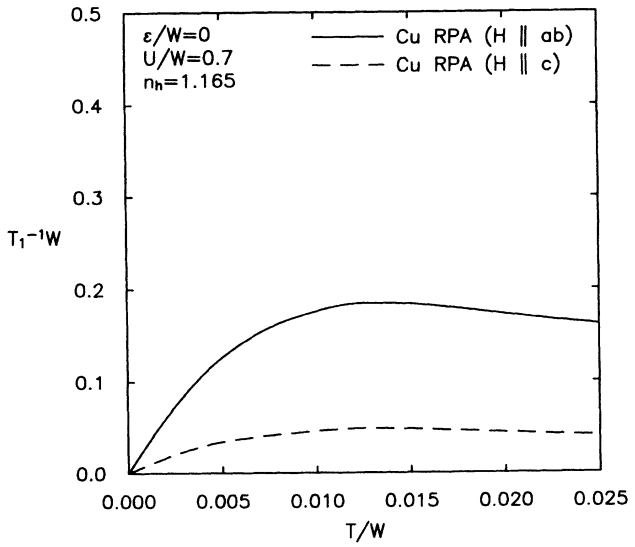

FIG. 14. Cu NMR for the anisotropic Mila-Rice relaxation mechanism. Nuclear relaxation rate T_1^{-1}, in units of $\pi(A^{zz})^2$. The assumed values of $a^{xx}=A^{xx}/|A^{zz}|$ and $b=B/|A^{zz}|$ are 4.7/227.7=0.02 and 40.7/227.7=0.18, respectively.

In the discussion up to this point, we have assumed hyperfine couplings to Cu($3d$) holes. If the dominant coupling at O or Y is nuclei is instead to O($2p\sigma$) holes, the RPA enhancements of T_1^{-1} which follow within our model are much less pronounced. In Fig. 15 the oxygen relaxation rate is plotted, assuming an isotropic coupling to $2p$ holes on nearest-neighbor O sites. In this case, K and T_1^{-1} are enhanced by roughly equal factors at low temperatures, and the resulting Korringa ratio is less than unity; further, the relaxation rate remains

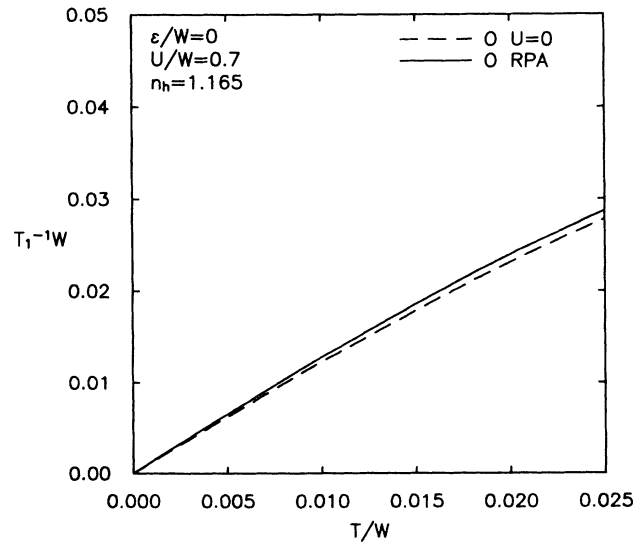

FIG. 15. O NMR for isotropic transferred hyperfine coupling to nearest-neighbor O spins in the CuO_2 model. Nuclear relaxation rate T_1^{-1}, in units of πA^2.

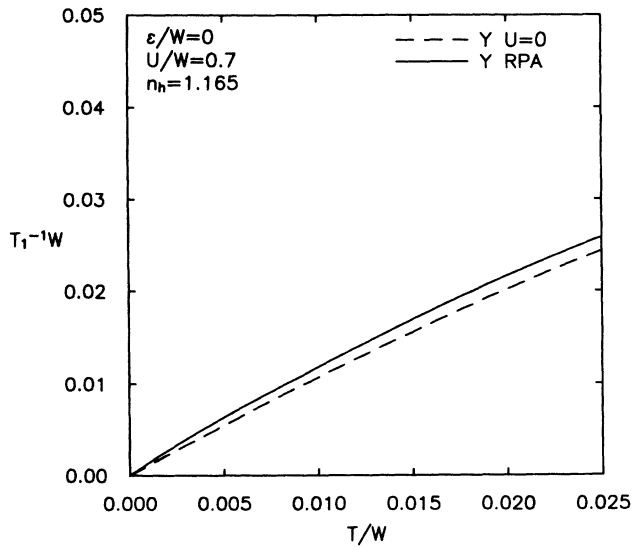

FIG. 16. Y NMR for isotropic transferred hyperfine coupling to nearest-neighbor O spins in the CuO_2 model. Nuclear relaxation rate T_1^{-1}, in units of πA^2.

Korringa-like over a larger temperature range. Similar behavior is exhibited for Y NMR (Fig. 16) if the dominant coupling is to the eight nearest-neighbor O sites.

V. CONCLUSIONS

The nature of the hole fluid in the layered cuprates remains an important open question. Here we have analyzed two limiting approximations, both based upon a hybridized Cu($3d$)-O($2p\sigma$) band with on-site Cu Coulomb interactions. The first proceeds from the insulating state in which the spin dynamics is described by a spin-$\frac{1}{2}$ Heisenberg model. Such a state is known to arise as an SDW or Mott-insulator limit of a half-filled Hubbard model, or possibly as a charge-transfer-insulator limit of the CuO_2 model. The effect of additional hole doping was modeled by cutting off the spin-spin correlation length[12] at a finite value l at low temperatures.

Using the expression for the dynamic spin structure factor obtained from a Schwinger boson (or a constrained spin-wave) approximation, we evaluated T_1^{-1} and K. Assuming an on-site hyperfine coupling, we found for the Cu sites that $T_1^{-1}\approx T^2\xi$, where $\xi\approx(J/T)e^{1.1J/T}$. For oxygen sites, we used a form factor that filters the large-q antiferromagnetic spin fluctuations and obtained a temperature dependence $T_1^{-1}\approx T^3$. From the dependence of T_1^{-1} on the electronic Zeeman frequency, which enters into our calculations as a cut off, we predicted that at high temperatures one will observe a magnetic field dependence for the relaxation rates. When holes are added and ξ is cut off by l, the relaxation rate at the Cu site can exhibit a weak maximum at lower temperatures, while the relaxation rate of the O site continues to fall as T^3. However, this requires a large value for l. Clearly the addition of doped holes does more to the spin dynamics than simply providing a limiting value for ξ. As suggested by various calculations,[30,31] one expects that the

added holes will lead to some type of quasi-particle spectral weight. Presumably the spin susceptibility associated with this part of the spectral weight gives rise to the Korringa-like behavior of T_1^{-1} observed on the O site and also modifies T_1^{-1} on the Cu sites.

The second approach we have discussed uses the RPA to model the dynamic spin susceptibility of a 2D Hubbard model and a 2D CuO_2 lattice. Again, the hyperfine form factors act to suppress the antiferromagnetic spin fluctuations at O sites, while leaving them at Cu sites. In addition, in the CuO_2 model the possibility of hyperfine couplings involving spins on the O sites was considered.

The form factors lead to an enhancement of T_1^{-1} on the Cu sites relative to the O sites. However, the O form factor which couples to the Cu sites in the analysis based on a 2D Hubbard model gives rise to a significant nonlinear T dependence of T_1^{-1} on the O site, which is not observed. This could simply be a consequence of the RPA, which leads to a spin fluctuation peak in $\chi(\mathbf{q})$ significantly displaced from (π,π). Alternatively, in the CuO_2 model with an on-site Cu Coulomb interaction, we find that if the O hyperfine coupling involves the four nearest-neighbor oxygens, a linear T dependence is obtained for T_1^{-1}. Similar results are found for the Y site. In both these models, the enhancement over the simple Korringa value of T_1^{-1} for Cu, at temperatures $T \sim 0.01W$, is of order what is observed.

Thus the qualitative picture in which antiferromagnetic fluctuations enhance the relaxation on the Cu site but are suppressed by the hyperfine form factors on the O and Y sites is clearly seen in both the limiting approximations we have studied. However, neither one provides a quantitative description of the doped materials.

Further insight is needed to describe the metallic systems. Among various features which remain to be resolved is the observed tracking of the T_1^{-1} rates of the Cu and O sites, which appears to set in at a characteristic temperature above the superconducting transition and continue through T_c to low temperatures.[6] Can this arise if the Cu hyperfine form factor supports the $\mathbf{q}^*=(\pi,\pi)$ Cu antiferromagnetic fluctuations while the O form factor suppresses the $\mathbf{q}^*=(\pi,\pi)$ antiferromagnetic contributions? In particular, will the ratio of these two rates remain fixed through T_c and down to low temperatures? Finally, it is clearly important to understand the behavior in the superconducting state, particularly as it provides direct information on the symmetry of the superconducting order parameter.[32]

Recently we received a preprint from F. Mila and T. M. Rice,[33] in which they have explored some of these physical ideas within the context of an anisotropic Heisenberg model.

ACKNOWLEDGMENTS

We want especially to thank D. J. Durand, P. C. Hammel, C. P. Slichter, M. Takigawa, R. E. Walstedt, and W. W. Warren for discussions of their data and ideas. We also want to acknowledge helpful discussions with F. J. Adrian and D. Cox. Finally, we hank H. Zhao for his assistance with the calculations performed at University of Southern California. N.E.B. and D.J.S. are grateful to the Institute for Theoretical Physics for its support during the high-T_c program under National Science Foundation Grant No. PHY82-17853, supplemented by funds from NASA. Partial support for this work was also provided by the National Science Foundation under Grant Nos. DMR86-15454 and DMR89-13850.

APPENDIX A

For the more general form factor $A^2(\mathbf{q})=A_0+A_1\gamma_{\mathbf{q}}+A_2\gamma_{\mathbf{q}}^2$ the nuclear relaxation rate T_1^{-1} within the Heisenberg model is given by

$$T_1^{-1}=\frac{2}{3\pi\eta^2 N}\sum_{\mathbf{k}}\frac{n_{\mathbf{k}}(n_{\mathbf{k}}+1)}{\omega_{\mathbf{k}}|\gamma_{\mathbf{k}}|}[A_0I_0(\mathbf{k})+A_1I_1(\mathbf{k})+A_2I_2(\mathbf{k})]\ , \tag{A1}$$

where

$$\begin{aligned} I_0(\mathbf{k})&=[1+(\omega_{\mathbf{k}}/\lambda)^2]K[(1-\gamma_{\mathbf{k}}^2)^{1/2}]\ ,\\ I_1(\mathbf{k})&=-\gamma_{\mathbf{k}}^2[1-(\omega_{\mathbf{k}}/\lambda)^2]K[(1-\gamma_{\mathbf{k}}^2)^{1/2}]\ ,\\ I_2(\mathbf{k})&=[1+(\omega_{\mathbf{k}}/\lambda)^2]\{D_1(\mathbf{k})K[(1-\gamma_{\mathbf{k}}^2)^{1/2}]\\ &\quad -D_2(\mathbf{k})E[(1-\gamma_{\mathbf{k}}^2)^{1/2}]\}\ , \end{aligned} \tag{A2}$$

with

$$\begin{aligned} D_1(\mathbf{k})&=\tfrac{1}{4}[1+\gamma_{2\mathbf{k}}(1+4\gamma_{\mathbf{k}}^2)-2\cos k_x\cos k_y]\ ,\\ D_2(\mathbf{k})&=\gamma_{2\mathbf{k}}-\cos k_x\cos k_y\ . \end{aligned} \tag{A3}$$

Here K and E are the complete elliptic integrals of the first and second kinds.

APPENDIX B

The transformation factors for computing partial susceptibilities of the noninteracting CuO_2 lattice [Eq. (4.6)] follow from a Green's function analysis. It is convenient to define the quantities

$$\begin{aligned} t_x(\mathbf{k})&=2t\cos(k_x/2)\ ,\\ t_y(\mathbf{k})&=2t\cos(k_y/2)\ ,\\ R(\mathbf{k})&=[(\tfrac{1}{2}\varepsilon)^2+t_x^2(\mathbf{k})+t_y^2(\mathbf{k})]^{-1/2}\ . \end{aligned} \tag{B1}$$

The diagonal factors α_{rr}^{ν} are squares of overlap matrix elements and may be interpreted as occupation probabilities; i.e., $\alpha_{rr}^{\nu}(\mathbf{k})$ is the probability that an electron with wave vector $\mathbf{k}$ and site index r lies in the ν-th band. This implies that

$$\sum_{\nu}\alpha_{rr}^{\nu}(\mathbf{k})=1\ . \tag{B2}$$

For the Cu sites,

$$\alpha_{dd}^{\pm}(\mathbf{k})=\tfrac{1}{2}[1\mp\tfrac{1}{2}\varepsilon R(\mathbf{k})]\ ,$$
$$\alpha_{dd}^{0}=0\ . \tag{B3}$$

(There is clearly no probability for a Cu hole to be in the nonbonding oxygen band.) For the type-a oxygen sites,

$$\alpha_{aa}^{\pm}(\mathbf{k})=\pm\tfrac{1}{2}\frac{t_x^2(\mathbf{k})R(\mathbf{k})}{E_{\mathbf{k}}^{\pm}-\varepsilon}\ ,$$
$$\alpha_{aa}^{0}(\mathbf{k})=1-[\alpha_{aa}^{+}(\mathbf{k})+\alpha_{aa}^{-}(\mathbf{k})]\ . \tag{B4}$$

For the type-b oxygen sites, the expressions are the same as in Eq. (B4), but with the replacements $a\rightarrow b$ and $x\rightarrow y$.

The off-diagonal factors $\alpha_{r'r}^{\nu}$ are products of distinct overlap matrix elements. Since the nonbonding oxygen band has no overlap with Cu orbitals, it follows immediately that

$$\alpha_{da}^{0}=\alpha_{ad}^{0}=\alpha_{db}^{0}=\alpha_{bd}^{0}=0\ . \tag{B5}$$

It may be verified that

$$\alpha_{da}^{\pm}(\mathbf{k})=\alpha_{ad}^{\pm}(\mathbf{k})=\mp t_x(\mathbf{k})R(\mathbf{k})\ . \tag{B6}$$

As before, expressions for α_{db} and α_{bd} follow from (B6) by letting $a\rightarrow b$ and $x\rightarrow y$. Finally, the off-diagonal factors involving oxygen orbitals are

$$\alpha_{ab}^{\pm}(\mathbf{k})=\alpha_{ba}^{\pm}(\mathbf{k})=\pm\tfrac{1}{2}\frac{t_x(\mathbf{k})t_y(\mathbf{k})R(\mathbf{k})}{E_{\mathbf{k}}^{\pm}-\varepsilon}\ ,$$
$$\alpha_{ab}^{0}(\mathbf{k})=\alpha_{ba}^{0}(\mathbf{k})=-[\alpha_{ab}^{+}(\mathbf{k})+\alpha_{ab}^{-}(\mathbf{k})]\ . \tag{B7}$$

[1]W. W. Warren, Jr., R. E. Walstedt, G. F. Brennert, G. P. Espinosa, and J. D. Remeika, Phys. Rev. Lett. **16**, 1860 (1987); R. E. Walstedt, W. W. Warren, Jr., R. F. Bell, G. F. Brennert, G. P. Espinosa, R. J. Cava, L. F. Schneemeyer, and J. V. Waszczak, Phys. Rev. B **38**, 9299 (1988).

[2]T. Imai, T. Shimizu, H. Yasuoka, Y. Ueda, and K. Kosuge, J. Phys. Soc. Jpn. **57**, 2280 (1988).

[3]C. H. Pennington, D. J. Durand, C. P. Slichter, J. P. Rice, E. D. Bukowski, and D. M. Ginsberg, Phys. Rev. B **39**, 2902 (1989).

[4]M. Takigawa, P. C. Hammel, R. H. Heffner, and Z. Fisk, Phys. Rev. B **39**, 7371 (1989).

[5]P. C. Hammel, M. Takigawa, R. H. Heffner, Z. Fisk, K. C. Ott, and J. D. Thompson (unpublished).

[6]P. C. Hammel, M. Takigawa, R. H. Heffner, Z. Fisk, and K. C. Ott, Phys. Rev. Lett. **63**, 1992 (1989).

[7]R. E. Walstedt, W. W. Warren, Jr., R. F. Bell, and G. P. Espinosa, Phys. Rev. B **40**, 2572 (1989).

[8]H. Alloul, T. Ohno, and P. Mendels, Phys. Rev. Lett. **63**, 1700 (1989).

[9]For a review, see R. J. Birgeneau and G. Shirane, in *Physical Properties of High Temperature Superconductors,* edited by D. M. Ginsberg (World Scientific, Singapore, 1989).

[10]S. Chakravarty, B. I. Halperin, and D. R. Nelson, Phys. Rev. Lett. **60**, 1057 (1988).

[11]S. Tyč, B. I. Halperin, and S. Chakravarty, Phys. Rev. Lett. **62**, 835 (1989).

[12]B. S. Shastry Phys. Rev. Lett. **63**, 1288 (1989).

[13]A. Auerbach and D. Arovas, Phys. Rev. Lett. **61**, 617 (1988); Phys. Rev. B **38**, 316 (1988).

[14]M. Takahashi, Phys. Rev. B **40**, 2494 (1989).

[15]J. E. Hirsch and S. Tang, Phys. Rev. B **39**, 2850 (1989); S. Tang, M. E. Lazzouni, and J. E. Hirsch (unpublished).

[16]F. J. Adrian, Phys. Rev. Lett. **61**, 2148 (1988).

[17]S. Chakravarty and R. Orbach (unpublished).

[18]T. Moriya, Prog. Theor. Phys. **28**, 371 (1962).

[19]V. Jaccarino, in *Proceedings of the International School of Physics, "Enrico Fermi," Course XVIII, Varenna, 1966* (Academic, New York, 1967).

[20]The constrained spin-wave approximation is not rotationally invariant, but the Schwinger boson theory (Ref. 13) is, as symmetry requires, and the dynamic form factor of that theory is exactly that of the longitudinal components, $\langle S^z(t)S^z(0)\rangle$, within the spin-wave theory. We therefore use that result for $S(\mathbf{q},\omega)$.

[21]F. Mila and T. M. Rice, Physica C **157**, 561 (1989).

[22]C. Scherer, J. E. Gulley, D. Hone, and V. Jaccarino, Rev. Brasil Fis. **4**, 299 (1974).

[23]S. Chakravarty, B. I. Halperin, and D. R. Nelson, Phys. Rev. B **39**, 2344 (1989).

[24]Independent evidence for the approximate validity of the spin wave $S(\mathbf{q},\omega)$ at $T=0$ lies in the exact numerical results of C.-X. Chen and H.-B. Schüttler, Phys. Rev. B **40**, 236 (1989), but it is dangerous to extrapolate this to $T>0$, where there is no long range order.

[25]The next-order term within these calculations is linear in T, in violation of the third law of thermodynamics, so we have not pursued further the details of the anticipated temperature dependence.

[26]H. J. Schultz (unpublished).

[27]For a 2D free-electron gas, the low-temperature momentum-dependent susceptibility is proportional to the density of states for $|\mathbf{q}|\leq 2p_F$. This implies that, within the RPA, the enhancement of T_1^{-1} is just equal to the square of the enhancement of the Knight shift, so that T_1TK^2 does not depend upon the on-site Coulomb interaction U. For a discussion see H. Nishihara, I. Shirotani, and N. Inoue, J. Phys. Soc. Jpn. **48**, 1957 (1980). Since in our analysis we treat the band structure within a tight-binding approximation, the susceptibility $\chi(\mathbf{q})$ peaks at large momentum. In this case T_1TK^2 depends upon U.

[28]T. Imai, T. Tsuda, H. Yasuoka, T. Takabatake, Y. Nakazawa, and M. Ishikawa (unpublished).

[29]T. Moriya and K. Ueda, Solid State Commun. **15**, 169 (1974).

[30]S. A. Trugman (unpublished).

[31]C.-X. Chen, H.-B. Schüttler, and A. J. Fedro (unpublished).

[32]H. Monien and D. Pines (unpublished).

[33]F. Mila and T. M. Rice (unpublished).